RESEARCH PAPER

Feature Selection and Masking in Mammograms for Breast Tumors Detection Using Convolution Neural Network

Ankit Mehto [a,*], Pritaj Yadav [b]

[a] Research Scholar (Department of Computer Science and Engineering, RNTU, Bhopal, 464993, India)

[b] Affiliation (Department of Computer Science and Engineering, RNTU, Bhopal, 464993, India)

*Corresponding Author E-mail : ankitmehto461@gmail.com

Abstract

This work presents a novel mammography-based method for detecting breast cancer that combines dimensionality reduction and feature extraction. A single representation is created by first extracting deep features from several convolutional neural network (CNN) models that have already been trained. Conventional machine learning classifiers are trained using this reduced feature set after the most informative features are chosen utilizing mutual information with the class labels. The proposed methodology is evaluated with four classifiers: support vector machine (SVM), random forest (RF), k-nearest neighbor (kNN), and neural network (NN). Among these, the NN classifier achieves the best performance, reaching 92% accuracy on the recently released RSNA dataset. This dataset includes two mammographic views and additional patient information, such as age, which contributes to the observed performance gains. Comparative experiments against leading methods show that the proposed algorithm provides superior accuracy and sensitivity. The method achieves 94.5% accuracy on the MIAS dataset and 96% accuracy on the DDSM dataset, underscoring its effectiveness for reliable breast lesion diagnosis and its advantage over existing techniques.

Keywords: Feature selection, Masking, Mammograms, Breast Cancer, CNN, ResNet18, ResNet34.

How to cite this article: Mehto A, Yadav P. Feature Selection and Masking in Mammograms for Breast Tumors Detection Using Convolution Neural Network. Int J Drug Deliv Technol. 2026;16(40s): 1061-1072. DOI: 10.25258/ijddt.16.40s.108

1. Introduction

Breast cancer (BC) remains one of the most widespread malignancies globally, contributing substantially to both incidence and mortality. In 2020, approximately 2.3 million new cases were reported, with an estimated 685,000 deaths attributed to the disease. Despite the reduction in death rates resulting from the adoption. The importance of routine mammography screening, coupled with early detection and timely treatment, continues to play a pivotal role in reducing breast cancer–related mortality rates [1-3]. Presently, the early identification of breast cancer from radiological images necessitates the proficiency of highly skilled radiologists. A forthcoming deficit of radiologists in multiple nations is expected to exacerbate this issue [4-6]. Mammography screening resulted in a significant occurrence of false positive outcomes. These factors may lead to additional imaging examinations, inconvenient follow-up visits, and unwarranted patient anxiety, in some cases, tissue sampling, typically via needle biopsy. In this regard, machine learning methods, especially graph-based clustering techniques, have demonstrated potential for enhancing the analysis of multiview radiological images [7–10]. Deep learning, a branch of machine learning, has lately altered how diagnostic imaging tests are interpreted [11]. The convolutional neural network (CNN) is a key component of deep learning architectures [12].

CNN-based computer-aided diagnostic (CAD) systems offer more rapid, reliable, and comprehensive screening than traditional techniques. CNNs have become a key tool for recognizing patterns in image analysis [13]. They are widely used in breast cancer detection across imaging techniques such as MRI, X-ray mammography, and ultrasound (US).

US images: A hybrid CNN-based method that diagnoses BC using ultrasound images was proposed in [14]. This system employed mRMR method for selection of feature to identify the most relevant features after extracting and concatenating features from ResNet50, MobileNetV2, and AlexNet. Machine learning algorithms were then used to train support vector machine (SVM) classifiers and k-nearest neighbor (k-NN).

Consequently, 95.6% accuracy was attained. An object recognition method involving feature classification, selection, and extraction was used in [15] to segment breast ultrasound (US) images into smaller sections and automatically identify those associated with breast cancer. Another approach [16] presented a semantic and patch merging classification-based method for segmenting images of breast cancer. This approach entails cropping a region of interest, improving it with filters and clustering algorithms, extracting features, and then classifying it using a a k-NN and neural network classifier.

X-ray images: A pre-trained convolutional neural network architectures are used in [17], namely ResNet50 and InceptionV3, to categorize mammographic cancers as benign or malignant using the DDSM dataset. The authors used transfer learning, data augmentation, and pre-processing, techniques to improve model performance because of the small dataset size. Among the two models, ResNet50 achieved the highest accuracy at 85.7%, while InceptionV3 attained 79.6%.

MRI images: A 3D deep CNN supervised learning is used for detecting and localizing breast cancer in MRI dynamic contrast-enhanced images in [18], achieving an accuracy of 83.7%. In another work [19], a multi-layer CNN utilizing online data augmentation and pixel-level information was introduced to classify MRI images as benign or malignant, reaching an accuracy of up to 98.33%.

A CNN model that combines data from numerous craniocaudal (CC) and mediolateral oblique (MLO) views was used by the authors in [20]. Using multi-scale features and a penalty term, the model's accuracy on the DDSM dataset was 82.02%. A BC detection technique based on the CBIS-DDSM image dataset was presented in [21]. Following image pre-processing, a number of CNN models, including and Inception ResNet, GoogLeNet, ResNet, VGG16, AlexNet, were used to extract features. A neural network classifier was then used to assess the extracted features, and it produced an accuracy of 88%.

Reducing false negatives is crucial for BC detection in order to guarantee correct diagnosis and avoid cases of missed positive cases that causes potential harm. In this work, we mainly concentrate on X-ray imaging datasets and offer a novel CNN-based technique to improve BC identification accuracy. By fixing the flaws in previous research, proposed method enhances overall detection performance drastically by reducing false negatives. Improving patient outcomes and advancing medical imaging diagnostics can be achieved by creating a more sophisticated and dependable breast cancer detection system.

There are two important contributions of the proposed work that enhanced the existing literature. First, it builds a feature vector by adding supplementary data, like age, and extracts a variety of features for various perspectives from multiple pre-trained CNNs. Second, it uses a dimensionality reduction technique that eliminates weak features according to how well they match the ground truth. There are 4 foundation models: ConvNeXtSmall, MobileNetSmall, ResNet50, and EfficientNet. For optimal classification, a model of NN is created by combining the properties of these models. This approach has the potential to improve BC categorization accuracy. The remaining paper is organized as follows: Section 2 describes the convolutional neural network; Section 3 presents the data set; Section 4 discusses the proposed methodology; Section 5 discusses the results on different datasets; followed by comparative analyses and conclusion in Section 6 and Section 7 respectively.

2. Convolutional Neural Network

One of the typical ANN that can handle input in a grid-like structure is the convolutional neural network, sometimes referred to as CNN or ConvNet. Unlike the net- work's name, which implies the mathematical operation known as convolution it does not precisely correspond to the definition as in engineering or pure mathematics [10-11]. Convolution or convolving is the process of scaling down the input without loss of information. It is built on the ideas of parameter sharing, sparsity of connections and backpropagation.

The history of ConvNets goes back to the late 1980s for the first time CNN is used to recognize handwritten zip codes sourced from the US Postal Service, thus creating LeNet. Due to the limitation of datasets and computational resources CNNs and the connectionism lost momentum until when [13] comes first in the Large-Scale ImageNet. ILSVRC-2012 Visual Recognition Challenge [14] contest using his new design AlexNet. With ConvNets becoming more popular, many attempts have been made by the community of computer vision that improve the performance of the original architecture resulting in ZFNet [15], GoogleNet [16], VGGNet [17], ResNet [18]. A concise summary of the different ConvNet architectures are tabulated in Table. I.

Table. I Popular CNN architectures [1]

Name	Ref.	Year	Layers	Contribution
AlexNet	[13]	2012	8	Fast feature extraction, data compression, SVM classifier.
ZFNet	[15]	2013	8	Visualization of deep features, invariance of features, evolution of features, and significance of features
GoogleNet	[16]	2014	22	Global average pooling, auxilary classifier
VGGNet	[17]	2014	19	Using ReLU, increased network depth
ResNet	[18]	2015	118	Introduction of residual network, skip connections

CNN is made up of several layers, fully connected layers, pooling, and including convolutional. The output of one layer is fed into the other sequentially. Apart from these three main components, the CNN also contain dropout layers and an output layer. Theselayers are briefly explained below:

1. Convolutional Layers: This layer is mainly used to perform the featuring extraction task. CNN takes an m × n image as input and slides the kernel weights or convolution filter of dimension f × f over the I/P image. The convolution operation involves the dot product sum of the kernel K and input I, where j and I are the indices. The resultant 2D output is called feature map or feature vector. Initially the kernel weights are initialized at random, then modified later throughout the training process. Figure 1(a) illustrates the convolution process.

2. Pooling Layer: This layer performs down-sample of the input feature vector without the loss of information. The Pooling layers are often affixed between convolutional layers to minimize the overall quantity of the parameters. The average, maximum, and minimum pooling methods are the most well-known and often used pooling algorithms. Figure 1(b) illustrates the maximum pooling operation.

3. Fully Connected Layer: This FC-layer forms the last few layers of the ConvNet. Much like the conventional neural networks, nodes in this mapping of all the activations of the layer that has be formed before in a mesh-like topology. This structure makes it easy to use matrix multiplication and bias offset to determine the activations.

Although convolutional neural networks have achieved great success, there are some inherent limitations. To obtain good performance, ConvNets require a huge amount of training data. Being a deep learning algorithm, the training process is time consuming and requires heavy computational power. In addition, annotated medical imaging datasets are scarce unlike the natural image.

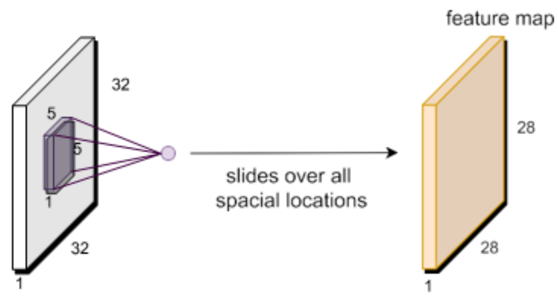

(a)

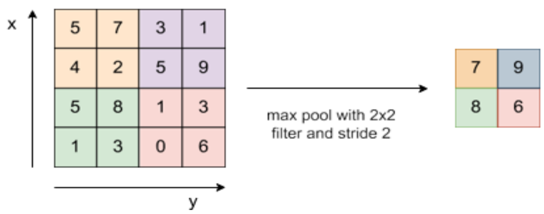

(b)

Figure 1 Operations in CNN Layers

3. Data Set

The North America Radiological Society dataset for this study was obtained from a recent Kaggle competition [22]. It includes 54,713 DICOM images collected from around 11,000 patients. At least four photos from various laterality and perspectives are available for every patient. Images from right and left laterality as well as two distinct viewpoints, CC and MLO, were supplied for every topic. The photographs come in a variety of sizes, styles, and formats, including monochrome-1 and monochrome-2, as well as jpeg and jpeg2000. The dataset offers additional variables, including age, implant, BIRADS, and density, some of which are useful for categorization. Although this dataset serves as the foundation for our study, it has not yet been utilized in any published studies due to its novelty. Therefore, we employ two more well-known datasets, MIAS and DDSM, for comparison. Any classification method is biased because only 2% of the images in our dataset are taken by cancer patients. To compensate for this imbalance, to compensate for this imbalance, we only employ 2,320 images from negative cases in addition to all available positive examples. Figure 2 Illustrative samples from the RSNA dataset showing image (a) with cancer, (b) a healthy.

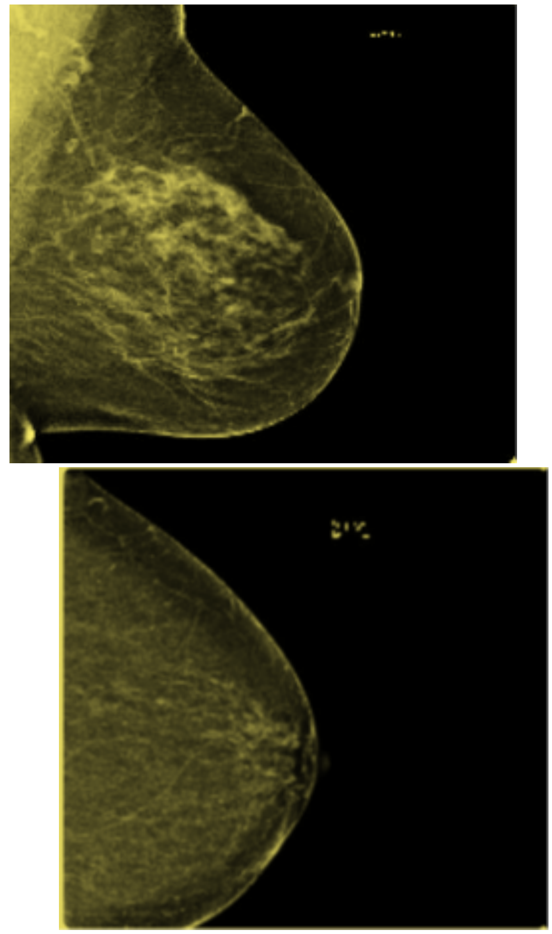

(a) (b)

Figure 2 Illustrative samples from the RSNA dataset showing image (a) with cancer, (b) a healthy subject

The Mammographic Image Analysis Society (MIAS) dataset [23] is a well-established benchmark frequently employed in the development and testing of computer-aided diagnosis (CAD) systems for breast cancer detection. It comprises 322 mammogram images, each accompanied by ground truth annotations that specify whether the detected abnormality is benign or malignant. Because the MIAS dataset encompasses both normal and abnormal mammograms, along with variations in breast tissue density and diverse lesion categories, it serves as a particularly valuable resource for researchers developing machine learning–based approaches to breast cancer detection. Its heterogeneity enables algorithms to be trained and evaluated across a broad spectrum of clinical scenarios. Figure 3 illustrates two representative samples from the collection, depicting a malignant case and a normal mammogram for comparison. Of the 55,890 photos in the DDSM [24], 86% are negative and 14% are positive. The pictures were shrunk to 299 × 299 after being tiled into 598 × 598 patches from a subset of this dataset known as CBIS-DDSM, experts have identified and separated regions of interest that correlate to positive cases. In this work, instead of using CBIS-DDSM, we use the original DDSM dataset to classify images from both healthy people and cancer patients. Two sample photos from this collection are shown in Figure 4 for both normal and cancerous instances. Table II compiles these three datasets.

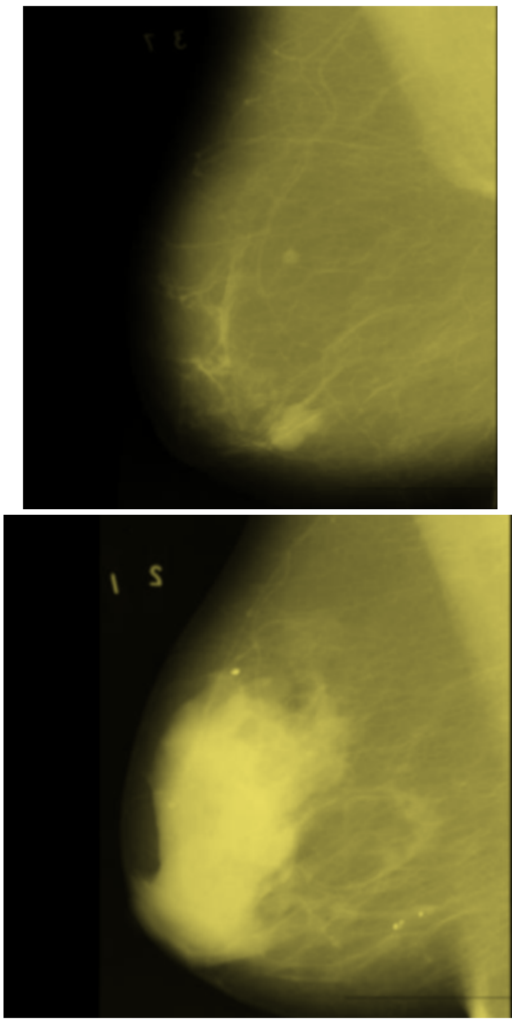

(a) (b)

Figure 3 Illustrative samples from the MIAS dataset showing image (a) with cancer, (b) a healthy subject

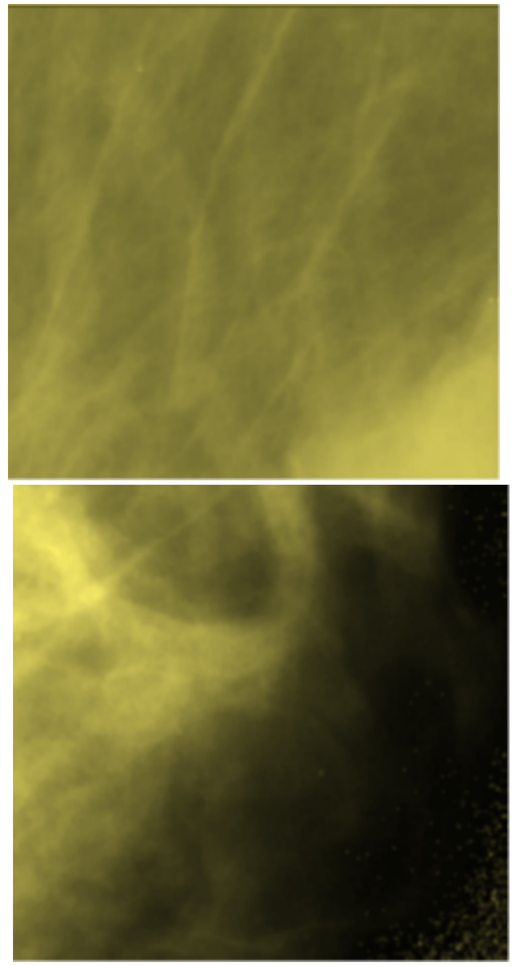

(a) (b)

Figure 4 Illustrative samples from the DDSM dataset showing image (a) with cancer, (b) a healthy subject

Table. II Details of datasets

ataset	No. of Images	Types of Images	Size of Image
DSM	55,890	JPGE	598×598
IAS	322	PGM	1024 × 1024
SNA	54,713	Variable	Variable

4. Proposed Methodology

In this study, we propose a methodology that leverages the concatenation and extraction of features from multiple convolutional neural network (CNN) architectures. The features obtained from these models are subsequently reduced, ensuring that the classification process between normal and malignant mammograms is driven exclusively by the most discriminative (positive) traits. Figure 5 depicts the general structure of the suggested system. As depicted, mammographic images from different datasets undergo preprocessing before being passed through several CNN models for feature extraction. The resulting feature sets are then subjected to dimensionality reduction; The refined features are then divided into two groups: cancer and non-cancer. Each block in the system architecture is explained in detail in the ensuing subsections [25].

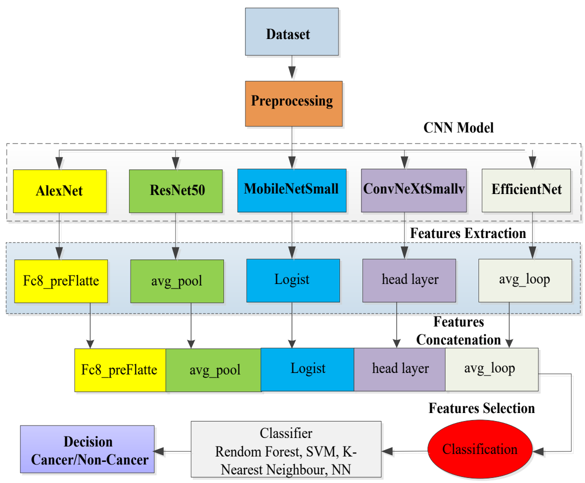

Figure 5: Block diagram of system under consideration.

Preprocessing: The photos used in this study come from different sources, and their resolutions and sizes vary.

Normalization: Mammography in different formats, such as 16-bit and 12-bit depth per pixel, are included in the RSNA collection. Furthermore, the dataset offers MONOCHROME1 and MONOCHROME2, two different photometric interpretations. Grayscale pixel values rise from bright to dark in the former, while they rise from dark to bright in the latter. All MONOCHROME1 photos are converted to the MONOCHROME2 format to provide uniformity throughout the dataset.

Following this conversion, intensity normalization is applied to standardize pixel values. Specifically, the values are rescaled to an 8-bit range (0–255), thereby producing uniform grayscale levels across the RSNA dataset. This normalization step enhances comparability between images and facilitates reliable feature extraction. By contrast, the DDSM and MIAS datasets already store mammograms in 8-bit format with pixel values ranging from 0 to 255. Consequently, no additional normalization is required for these datasets, as their pixel intensity distributions are already suitable for subsequent processing [26].

The mammography image is first subjected to a global thresholding procedure in order to identify the breast region for additional analysis. The largest connected item in the picture, which corresponds to the breast region, may be identified thanks to this step. The contour of this object is then extracted and used for obtaining a binary mask. By applying this mask, the images are cropped to retain only the relevant breast tissue, thereby defining the specific region of interest for subsequent examination and feature extraction.

Image Alignment: There are two different laterality groups in breast cancer datasets: left and right. We orient all laterality labels to the left in order to increase analysis accuracy and consistency. To provide a consistent orientation throughout the datasets, all left breast photos are flipped horizontally. We provide a dependable and consistent dataset for additional investigation and analysis by standardizing the laterality representation [27].

Feature extraction: The generated features by pretrained convolutional neural network (CNN) models, as outlined in Section 2.2. For each network, feature extraction is performed at the penultimate layer, i.e., the layer immediately preceding the final fully connected (FC) layer. The final FC layer's output is explicitly trained on the 1000 ImageNet classes, which have nothing to do with the mammography domain, which is why this decision was made. By bypassing this layer, we obtain more generalizable representations that capture high-level image characteristics without being biased toward ImageNet categories.

Table III summarizes the specific penultimate layers utilized for each CNN model in this study, along with the dimensionality of the extracted feature vectors. These features serve as the foundation for subsequent dimensionality reduction and classification tasks.

Feature concatenation: To construct a unified representation, the one-dimensional (1D) feature vectors obtained in the preceding stage are concatenated into a single composite feature vector. It is crucial to remember that characteristics are taken from two different mammography perspectives for each CNN model: cranio-caudal (CC) and medio-lateral oblique (MLO). By combining the features from both views, the resulting vector captures complementary information, thereby enhancing the discriminative power of the representation for subsequent classification tasks. Ten 1D vectors are thus concatenated in this instance. This creates a vector that is 18,384 in size. We have an extra helpful characteristic for the patient age in the RSNA dataset that serves as the foundation for our study. The RSNA dataset's age feature distribution for both cancer and non-cancer participants is shown in Figure 6. As is evident, aging can also be regarded as a desirable characteristic. By normalizing the concatenated feature vectors and incorporating patient age as an additional attribute, the final representation comprises a total of 18,385 features.

Feature selection: Most of the extracted features are redundant, offering little discriminative value and unnecessarily increasing system complexity. Figure 7 provides examples of both informative and non-informative features. As shown, weak features exhibit similar distributions for malignant and normal cases, resulting in zero mutual information and thus contributing no useful knowledge to the classification process. In contrast, strong features display clear differences in distribution between the two classes, indicating that they contain modest yet meaningful information capable of improving the performance of classifiers in the subsequent stage. We employ the method in [28] to calculate mutual information. Empirically, we discovered that a threshold of 0.02 yields the best outcomes. It is important to highlight that a range of feature selection strategies were employed in this study, with mutual information serving as the primary criterion for empirical evaluation. Table IV displays the number of features retained for each dataset both after and before feature selection is used.

Classification of characteristics: By selecting the most informative features, we proceed to their classification. Several machine learning algorithms were evaluated, including k-Nearest Neighbors (k-NN), Random Forest (RF), Support Vector Machine (SVM), and Neural Networks (NN). In our experiments, the RF classifier demonstrated superior performance when configured with specific parameters: an ensemble of 100 trees, a maximum of five features taken into account per tree, two samples needed to divide a node, and a maximum tree depth of four. These parameter settings were chosen to optimize diagnostic accuracy and enhance breast cancer detection in the mammographic datasets.

With the regularization value C=1, we used a linear kernel for the SVM classifier. This choice balances training accuracy with decision boundary complexity, while the linear kernel facilitates learning a linear separation between classes.

Two fully connected (FC) layers were used to create the NN classifier: a final single-neuron output layer for binary classification and a hidden layer of 96 neurons. In order to ensure classification based on the majority vote among the five nearest neighbours, the kNN classifier was finally set to k=5. We employ a sigmoid activation function for the classification layer, which distinguishes between malignant and non-cancerous cases

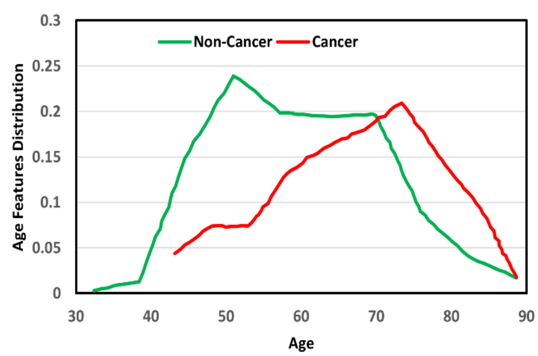

Figure 6: Illustrative age distribution of RSNA dataset for cancer and noncancer.

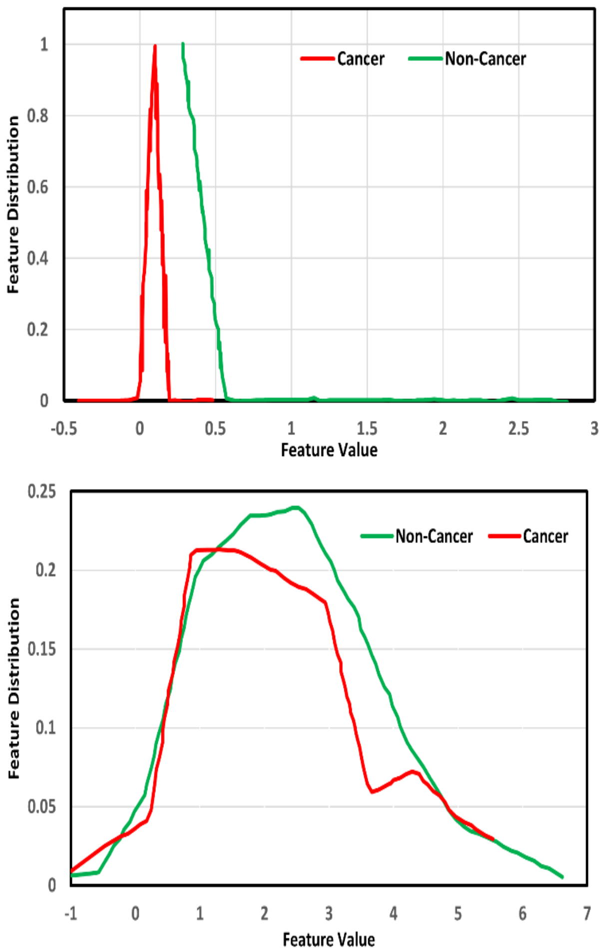

(a)

(b)

Figure 7: shows two CNN-extracted features for cancer and non-cancer cases in the DDSM dataset. Feature (a) is informative, with better class separation and a mutual information of 0.035. Feature (b) shows strong overlap and has zero mutual information, indicating it provides no useful information for classification.

Table. III Description of CNN model Used

Layer Name	CNN Models	No. of Features
avg_pool	EfficientNet	1280
head_layer	ConvNeXtSmall	768
fc8_preflatten	AlexNet	4096
Logits	MobileNetSmall	1000
avg_pool	ResNet50	2048

Table. IV Total datasets obtained

Dataset	Before Feature Selection	After Feature Selection
DDSM	9192	206
MIAS	9192	212
RSNA	18,385	452

5. Results Analysis

This section includes a synthesis of all datasets, as well as the results obtained from the three datasets described using the models presented in Section 3. For every dataset, we used k-fold cross-validation. where k is equal to 10. Using 90% of the data for training and 10% of the data for testing, the method was trained and tested ten times.

Table V examines the performance characteristics of several CNN models using the RSNA dataset. In terms of precision, sensitivity, accuracy, F-Score, and AUC, EfficientNet routinely performs better than the other CNN models. Its architecture, which allows it to gather pertinent data and generate precise predictions on the RSNA dataset, is responsible for its extraordinary performance. When it comes to correctly categorizing medical images in the RSNA dataset, EfficientNet outperforms all other models. The final row of the table illustrates how each performance parameter is much enhanced by the suggested concatenation method. For example, the accuracy achieved is 6% higher than the best CNN model, EfficientNet.

Table. V Performance evaluation for RSNA dataset with NN

Different Models	Pr(%)	Sn(%)	Acc(%)	F-score	AUC
EfficientNet	88	92	86	0.90	0.92
ConvNeXtSmall	83	87	79	0.85	0.83
AlexNet	87	87	81	0.86	0.82
MobileNetSmall	81	85	77	0.83	0.81
ResNet50	86	90	84	0.88	0.89
Proposed Model	92	96	92	0.94	0.96

The results employing the kNN classifier with k = 5 are summarized in Table VI. When compared to the NN model, the results demonstrate a significant decline in performance. In particular, the maximum accuracy is obtained without feature concatenation with AlexNet, which is 13% less accurate as the top-performing. The EfficientNet model is 8% less accurate. Additionally, the preciseness of the concatenated model employing with neural network NN classifier is 14% higher than that of the concatenated model.

Table. VI Performance evaluation for RSNA dataset with KNN

CNN Models	Pr(%)	Sn(%)	Acc(%)	F-score	AUC
EfficientNet	74	78	73	0.72	0.75
ConvNeXtSmall	70	74	62	0.67	0.67
AlexNet	72	70	71	0.68	0.68
MobileNetSmall	67	71	60	0.65	0.64
ResNet50	71	75	69	0.68	0.71
Proposed Model	79	81	78	0.78	0.80

The outcomes of the suggested approach utilizing the SVM classifier are shown in Table VII. The table makes it clear that, out of the four techniques examined, SVM has the lowest accuracy. In particular, the SVM-based approach's accuracy is 19% less than that of the NN-based approach. Additionally, the concatenated model's accuracy dropped by 5% when compared to the KNN and RF-based systems.

Table. VII Performance evaluation for RSNA dataset with RF

CNN Models	Pr(%)	Sn(%)	Acc(%)	F-score	AUC
EfficientNet	66	70	68	0.68	0.68
ConvNeXtSmall	61	65	62	0.63	0.63
AlexNet	63	61	62	0.62	0.62
MobileNetSmall	59	63	60	0.61	0.60
ResNet50	63	66	64	0.64	0.65
Proposed Model	72	75	73	0.73	0.74

6. Comparative Analysis

The findings displayed in Tables IV–VII make it evident that the NN classifier achieves optimal performance. We employed the set value to evaluate the suggested strategy with the existing techniques. To the best of our knowledge, no previously published works have made use of the RSNA dataset. As a result, we used the MIAS and DDSM datasets to compare our suggested model with current approaches for the purposes of this section, and Table VIII summarizes the findings. On the MIAS and DDSM datasets, it is evident that our proposed model has outperformed state-of-the-art algorithms in terms of accuracy and sensitivity. Our system outperformed the other two performance criteria, even though the approach outlined in [29] showed considerably higher precision for the MIAS dataset.

Table. VIII Comparison of model performance with experts

Method	**Number of Images**	**Dataset**	**Pr (%)**	**Sn (%)**	**ACC (%)**
CNNs [29]	11,218	MIAS & InBreast	86.59	82.28	85.82
CNN [30]	10,480	MIAS	NA	NA	93.5
CNN-4d [31]	547	Mini-MIAS dataset	83.67	90.63	89.05
Voting Classifier [32]	322	Mini-MIAS	NA	NA	85
KNN [33]	120	MIAS	NA	NA	92
GMM & SVM [34]	90	Mini-MIAS	NA	NA	92.5
LQP & SVM [35]	95	DDSM	NA	NA	94
SVM & Hough [36]	322 &206	DDSM	92.81	80.67	86.13
Our Method + NN	55890	DDSM	97	94.70	96

Our Method + NN	322	MIAS	91.80	96.32	94.5
Our Method + NN	54,713	RSNA	92	96	92

7. Conclusion

In order to accurately diagnose breast cancer using mammography images, we have created a new technique. In our method, features are extracted and chosen from many pre-trained CNN models, and then different machine learning algorithms-NN, RF, SVM, and kNN, are used for classification. The outcomes for several datasets show how successful our suggested plan. After analyzing the results, it is observed that the best results in the proposed method. Specifically, for the DDASM, MIAS, RSNA, and datasets, we attained remarkable accuracies of 96%, 94.5%, and 92%, respectively. These outcomes outperform those of current techniques, highlighting the superiority of our method in terms of sensitivity and accuracy.

We hope to improve our approach in a number of ways in the future. First, investigating cutting-edge deep learning methods like attention mechanisms could enhance the model's functionality even more. Second, looking into the incorporation of more genetic and clinical data may improve our system's precision and prediction power. Last but not least, thorough validation on bigger datasets from other healthcare facilities would offer stronger proof of the method's efficacy and generalizability.

Funding Information

No funding was received for this study.

Conflict of Interest

The authors declare that they have no known competing financial interests or personal relationships that could have appeared to influence the work reported in this paper.

Author's contribution

The authors confirm sole responsibility for the conception, design, analysis, and preparation of this manuscript.

Other Ethics Statements

All data generated or analyzed during this study are included in this published article. No additional datasets were used.

References

[1] Kim, J., Harper, A., McCormack, V., Sung, H., Houssami, N., Morgan, E., ... & Fidler-Benaoudia, M. M. (2025). Global patterns and trends in breast cancer incidence and mortality across 185 countries. Nature medicine, 31(4), 1154-1162. https://doi.org/10.1038/s41591-025-03502-3

[2] Xiong, X., Zheng, L. W., Ding, Y., Chen, Y. F., Cai, Y. W., Wang, L. P., ... & Yu, K. D. (2025). Breast cancer: pathogenesis and treatments. Signal transduction and targeted therapy, 10(1), 49. https://doi.org/10.1038/s41392-024-02108-4.

[3] Jafari, Z., & Karami, E. (2023). Breast cancer detection in mammography images: a CNN-based approach with feature selection. Information, 14(7), 410. https://doi.org/10.3390/info14070410.

[4] Liao, Q. M., Hussain, W., Liao, Z. X., Hussain, S., Jiang, Z. L., Zhu, Y. H., ... & Wu, D. D. (2025). Computer-Aided Application in Medicine and Biomedicine. International Journal of Computational Intelligence Systems, 18(1), 221. https://doi.org/10.1007/s44196-025-00936-y.

[5] Marcon, M., Fuchsjäger, M. H., Clauser, P., & Mann, R. M. (2024). ESR Essentials: screening for breast cancer-general recommendations by EUSOBI. European Radiology, 34(10), 6348-6357. https://doi.org/10.1007/s00330-024-10740-5.

[6] Apesteguía, L., & Pina, L. J. (2011). Ultrasound-guided core-needle biopsy of breast lesions. *Insights into imaging*, *2*(4), 493-500. https://doi.org/10.1007/s13244-011-0090-7.

[7] Zhang, C., Xu, D., Chen, C., Zhang, M., & Li, H. (2025). Multi-relational multi-view clustering and its applications in cancer subtype identification. *Information Fusion*, *117*, 102831. https://doi.org/10.1016/j.inffus.2024.102831.

[8] Wang, H., Yao, M., Chen, Y., Xu, Y., Liu, H., Jia, W., ... & Wang, Y. (2024). Manifold-based incomplete multi-view clustering via bi-consistency guidance. IEEE Transactions on Multimedia, 26, 10001-10014. doi: 10.1109/TMM.2024.3405650.

[9] Yao, M., Wang, H., Chen, Y., & Fu, X. (2024). Between/within view information completing for tensorial incomplete multi-view clustering. IEEE

transactions on multimedia, 27, 1538-1550. doi: 10.1109/TMM.2024.3521771.

[10] Bian, J., Xie, X., Lai, J. H., & Nie, F. (2024). Multi-view contrastive clustering via integrating graph aggregation and confidence enhancement. Information Fusion, 108, 102393. https://doi.org/10.1016/j.inffus.2024.102393.

[11] Luo, L., Wang, X., Lin, Y., Ma, X., Tan, A., Chan, R., ... & Chen, H. (2024). Deep learning in breast cancer imaging: A decade of progress and future directions. IEEE Reviews in Biomedical Engineering. doi: 10.1109/RBME.2024.3357877.

[12] Zhao, X., Wang, L., Zhang, Y., Han, X., Deveci, M., & Parmar, M. (2024). A review of convolutional neural networks in computer vision. Artificial Intelligence Review, 57(4), 99. https://doi.org/10.1007/s10462-024-10721-6.

[13] Emam, M. M., Houssein, E. H., Samee, N. A., Alohali, M. A., & Hosney, M. E. (2024). Breast cancer diagnosis using optimized deep convolutional neural network based on transfer learning technique and improved Coati optimization algorithm. Expert Systems with Applications, 255, 124581. https://doi.org/10.1016/j.eswa.2024.124581.

[14] Sahu, A., Das, P. K., & Meher, S. (2023). High accuracy hybrid CNN classifiers for breast cancer detection using mammogram and ultrasound datasets. Biomedical Signal Processing and Control, 80, 104292. https://doi.org/10.1016/j.bspc.2022.104292.

[15] Li, J., Song, L., Liu, X., Liu, Y., Ma, T., Bai, J., ... & Xu, X. (2026). Research on breast ultrasound images lesion localization and diagnosis based on knowledge-driven and data-driven methods. Computers in Biology and Medicine, 203, 111465. https://doi.org/10.1016/j.compbiomed.2026.111465.

[16] Fu, L., Li, N., Liao, Z., Lin, Y., Li, Z., & Li, F. (2026). Advances in Breast Ultrasound Segmentation and Classification. *Advanced Ultrasound in Diagnosis and Therapy*, *10*(1), 29-41. https://doi.org/10.26599/AUDT.2026.250056.

[17] Wang, L. (2024). Mammography with deep learning for breast cancer detection. Frontiers in oncology, 14, 1281922. https://doi.org/10.3389/fonc.2024.1281922.

[18] Di Piazza, T., Lazarus, C., Nempont, O., & Boussel, L. (2025, April). Leveraging clinical indications and demographics to improve multilabel abnormality classification in 3D chest CT scans. In Medical Imaging 2025: Computer-Aided Diagnosis (Vol. 13407, pp. 138-145). SPIE. https://doi.org/10.1117/12.3046901.

[19] Mehto, A., & Yadav, P. (2025, November). Masking in Mammograms for Breast Tumors Detection using CNN. In 2025 IEEE Silchar Subsection Conference (SILCON) (pp. 1-5). IEEE. doi: 10.1109/SILCON67893.2025.11327337.

[20] Sun, L., Wang, J., Hu, Z., Xu, Y., & Cui, Z. (2019). Multi-view convolutional neural networks for mammographic image classification. IEEE Access, 7, 126273-126282. doi: 10.1109/ACCESS.2019.2939167.

[21] Aguerchi, K., Jabrane, Y., Habba, M., & El Hassani, A. H. (2024). A CNN hyperparameters optimization based on particle swarm optimization for mammography breast cancer classification. Journal of imaging, 10(2), 30. https://doi.org/10.3390/jimaging10020030.

[22] Gupta, N., Kubicek, J., Penhaker, M., & Derawi, M. (2025). A novel diagnostic framework for breast cancer: Combining deep learning with mammogram-DBT feature fusion. Results in Engineering, 25, 103836. https://doi.org/10.1016/j.rineng.2024.103836.

[23] Suckling, J., Parker, J., Dance, D., Astley, S., Hutt, I., Boggis, C., ... & Savage, J. (2015). Mammographic image analysis society (mias) database v1. 21. https://doi.org/10.17863/CAM.105113.

[24] Ribli, D., Horváth, A., Unger, Z., Pollner, P., & Csabai, I. (2018). Detecting and classifying lesions in mammograms with deep learning. Scientific reports, 8(1), 4165. https://doi.org/10.1038/s41598-018-22437-z.

[25] Krizhevsky, A., Sutskever, I., & Hinton, G. E. (2012). Imagenet classification with deep convolutional neural networks. Advances in neural information processing systems, 25. https://proceedings.neurips.cc/paper_files/paper/2012/file/c399862d3b9d6b76c8436e924a68c45b-Paper.pdf.

[26] Li, Y. (2022, January). Research and application of deep learning in image recognition. In 2022 IEEE 2nd international conference on power, electronics and computer applications (ICPECA) (pp.

994-999). IEEE. doi: 10.1109/ICPECA53709.2022.9718847.

[27] Tan, M., & Le, Q. (2021, July). Efficientnetv2: Smaller models and faster training. In International conference on machine learning (pp. 10096-10106). PMLR. http://proceedings.mlr.press/v139/tan21a/tan21a.pdf.

[28] Qin, D., Leichner, C., Delakis, M., Fornoni, M., Luo, S., Yang, F., ... & Howard, A. (2024, September). MobileNetV4: Universal models for the mobile ecosystem. In European conference on computer vision (pp. 78-96). Cham: Springer Nature Switzerland. https://doi.org/10.1007/978-3-**031-736**61-2_5.

[29] Shiri, F. M., Perumal, T., Mustapha, N., & Mohamed, R. (2023). A comprehensive overview and comparative analysis on deep learning models: CNN, RNN, LSTM, GRU. arXiv preprint arXiv:2305.17473. https://doi.org/10.48550/arXiv.2305.17473.

[30] Zheng, J., Lin, D., Gao, Z., Wang, S., He, M., & Fan, J. (2020). Deep learning assisted efficient AdaBoost algorithm for breast cancer detection and early diagnosis. Ieee Access, 8, 96946-96954. doi: 10.1109/ACCESS.2020.2993536.

[31] Li, B., Ge, Y., Zhao, Y., Guan, E., & Yan, W. (2018, February). Benign and malignant mammographic image classification based on convolutional neural networks. In Proceedings of the 2018 10th International Conference on Machine Learning and Computing (pp. 247-251). https://doi.org/10.1145/3195106.3195163

[32] Agrawal, S., Rangnekar, R., Gala, D., Paul, S., & Kalbande, D. (2018, January). Detection of breast cancer from mammograms using a hybrid approach of deep learning and linear classification. In 2018 International Conference on Smart City and Emerging Technology (ICSCET) (pp. 1-6). IEEE. doi: 10.1109/ICSCET.2018.8537250.

[33] Diaz, R. A. N., Swandewi, N. N. T., & Novianti, K. D. P. (2019, August). Malignancy determination breast cancer based on mammogram image with k-nearest neighbor. In 2019 1st international conference on cybernetics and intelligent system (ICORIS) (Vol. 1, pp. 233-237). IEEE. doi: 10.1109/ICORIS.2019.8874873.

[34] Arafa, A. A. A., El-Sokary, N., Asad, A., & Hefny, H. (2019). Computer-aided detection system for breast cancer based on GMM and SVM. Arab Journal of Nuclear Sciences and Applications, 52(2), 142-150.

[35] Vijayarajeswari, R., Parthasarathy, P., Vivekanandan, S., & Basha, A. A. (2019). Classification of mammogram for early detection of breast cancer using SVM classifier and Hough transform. Measurement, 146, 800-805. https://doi.org/10.1016/j.measurement.2019.05.083.

[36] Rampun, A., Scotney, B. W., Morrow, P. J., Wang, H., & Winder, J. (2018). Breast density classification using local quinary patterns with various neighbourhood topologies. Journal of Imaging, 4(1), 14. https://doi.org/10.3390/jimaging4010014.